European Journal of Applied Physics
ISSN: 2684-4451

Predominant Scattering Mechanisms in Quaternary AlInGaN/GaN Heterostructures

Remziye Tülek, Sibel Gökden, Ali Teke, Engin Arslan, and Ekmel Özbay

***Abstract* — Scattering mechanisms that limit the mobility of two-dimensional electron gas (2DEG) in AlInGaN/GaN heterojunctions with three different barrier layer thicknesses of 37.2 (sample A), 10.6 (sample B) and 4.30 (sample C) nm were studied. Hall measurements were performed between 12 and 350 K. Mobilities limited by scattering due to acoustic and optic phonons, dislocation, interface roughness, and alloy disorder were used in the calculation. It was found that scattering, predominantly due to interface roughness, determine the Hall mobility for all samples at different strengths. The highest electron mobility of 492 $cm^2V^{-1}s^{-1}$ at room temperature is obtained for sample B with a high sheet density of about 4.43×10^{13} cm^{-2} and a corresponding sheet resistance of 287 Ω.**

***Keywords* —** AlInGaN/GaN, Interface Roughness Scattering, Transport.

I. Introduction

Due to the need for improved performance in higher frequency and high-power microwave applications, different barrier/channel alternatives have been implemented in nitride-based polarization-induced two-dimensional electron gas (2DEG). [1]-[6]. The conventional structure usually consists of a thick layer of GaN channel and a thin layer of AlGaN barrier with, possibly, a thin layer of AlN spacer at the interface [7]-[10]. Mobility and carrier density are key parameters for higher device performance. In the literature, many studies have been carried out to improve these two parameters by using lattice-matched or slightly mismatched AlInN [11]-[16] as a barrier, and a thin layer of InGaN [17]-[20] or dual channel configurations as a channel [21]-[23]. Quaternary AlInGaN layers have recently been introduced as an alternative barrier in nitride-based heterostructures [24]-[36]. Since AlInGaN quaternary alloys are expected to have narrower immiscibility gaps compared to their ternary counterparts other than AlGaN [10], higher mobilities can be realized in such structures. In addition, lattice constants and band gap energies of barrier layer can be more freely controlled by adjusting the alloy composition to reduce the strain-induced defect densities and thus improve the device performance [36]. The reported electron mobilities of AlInGaN/GaN heterostructures with different alloy compositions vary widely from 689 to 2200 $cm^2V^{-1}s^{-1}$ [37], [38]. As the transport properties are closely related to growth parameters and design of layered structure, their optimization should be addressed systematically as needed. Therefore, it is important to understand the scattering processes that limit the electron mobility of these heterostructures. Scattering due to alloy disorder in quaternary barrier structures is expected to be the dominant mechanism determining the transport properties of AlInGaN/GaN HEMTs. Similarly, relatively large differences in growth temperatures optimized for the channel and barrier/spacer layers, with possible growth interruption, could distort the surface morphology and subsequently restrict the mobility through interface roughness scattering. For samples with higher sheet carrier densities, the scattering is even more severe. Therefore, to achieve higher mobility in AlInGaN/GaN heterostructures, improvement and control of the interface qualities should also be considered.

This study is dedicated to investigating the transport properties of a relatively low interface quality AlInGaN/GaN heterojunction using temperature-dependent (12-350 K) Hall effect measurements. Three samples referred as A, B, and C with nearly the same alloy compositions (AlInGaN) but different barrier thicknesses were grown on sapphire substrate by Metal Organic Chemical Vapor Depositions (MOCVD).

Submitted on November 05, 2022.
Published on December 09, 2022.
R. Tülek, Department of Physics, Balıkesir University, Turkey.
(corresponding e-mail: baran@balikesir.edu.tr)
S. Gökden, Department of Physics, Balıkesir University, Turkey.
(e-mail: sibelgokden@gmail.com)
A. Teke, Department of Physics, Balıkesir University, Turkey.
(e-mail: ateke@balikesir.edu.tr)
E. Arslan, Department of Electrical and Electronics Engineering, Antalya Bilim University, Turkey.
(e-mail: engin.arslan@antalya.edu.tr)
E. Özbay, Department of Physics, Bilkent University, Turkey.
(e-mail: ozbay@bilkent.edu.tr)

Alloy compositions, layer thicknesses, dislocation densities, and interface and structural parameters were extracted from X-ray photoelectron spectroscopy (XPS), high resolution x-ray diffraction (HR-XRD), scanning electron microscope (SEM), and atomic force microscope (AFM) measurements. The results from these measurements were used to calculate the scattering-limited mobilities mainly due to optical phonon, acoustic phonon, interface roughness, dislocation, and alloy disorder. These calculated mobilities were applied to the Hall data taken in the 12-350 K temperature range to analyze the transport properties and identify the prominent scattering mechanisms.

II. Experimental Details

Three $Al_xIn_yGa_{1-x-y}N$/GaN heterojunctions were grown on (0001) sapphire substrates in a low-pressure MOCVD reactor. Triethylgallium (TEGa), trimethylaluminum (TMAl), trimethylindium (TMIn), and ammonia were used as Ga, Al, In, and N precursors, respectively. All samples were grown under the same growth conditions except for the thicknesses of barrier layer, following the procedure given below. The surfaces of the substrates were first prepared for growth by baking under H_2 ambient at 1150°C for 10 min. A low-temperature GaN (LT-GaN) buffer layer with a thickness of about 50 nm was grown on baked surfaces at 515°C. Growth of the GaN template layer was carried out in two stages under different growth conditions. First, 1 µm thick high-temperature GaN (HT-GaN) template layers were grown at 1040°C and 300 mbar. Additional layers of undoped HT-GaN nominally 2 µm thick were deposited at 1060°C and 150 mbar as a second part of the GaN template layer. The growths were completed by growing the $Al_xIn_yGa_{1-x-y}N$ barrier layers at 1150°C and 30 mbar.

Prior to device fabrication, the $Al_xIn_yGa_{1-x-y}N$ epilayer thicknesses were found out by SEM images. Similarly, the molar fractions of In, Al, and Ga in the $Al_xIn_yGa_{1-x-y}N$ epilayers and structural properties of samples were obtained from XPS and HR-XRD measurements. The surface morphologies of $Al_xIn_yGa_{1-x-y}N$ epilayers were obtained by AFM run in contact mode.

After characterization, the wafers were cut into several 8x8 mm pieces to provide ohmic contact formation on samples in Van Der Pauw geometry. Before fabrication, all samples were subjected to the following surface cleaning processes given below. First, the samples were placed in acetone in an ultrasonic bath for surface cleaning. The samples removed from the ultrasonic bath were immersed in isopropyl alcohol and rinsed in 18 MΩ resistive deionized (DI) water. The cleaned samples were placed in HC_l:H_2O (1:1) solution for 30 seconds to remove surface oxides and then rinsed again in DI water for a certain period of time. Ohmic contacts were obtained by depositing Ti/Al/Ni/Au (45/120/55/300 nm) on the $Al_xIn_yGa_{1-x-y}N$ surface and then annealing at 800°C in N_2 environment for 45 sec. The final structure of device is shown schematically in Fig. 1.

Temperature-dependent Hall measurements were done for all samples in the temperature range of 12-350 K with a sensitivity better than ± 0.1 K. Carrier mobilities and densities were deduced from the Hall data at each temperature. By using these Hall data in conjunction with other data obtained from the above-mentioned measurements, the transport properties of the samples were determined and evaluated in the light of analytical calculations.

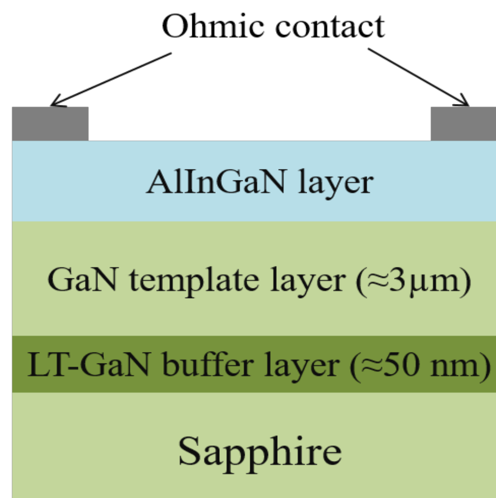

Fig. 1. The schematic representation of AlxInyGa1-x-yN/GaN heterojunction grown on sapphire substrate.

III. Experimental Results and Calculations

Surface quality and morphology of $Al_xIn_yGa_{1-x-y}N$ epilayers was examined by optical microscopy and AFM imaging. It was determined from the optical microscope image that the surfaces of the samples were crack-free and in a mirror-like form. As shown in Fig. 2, the AFM images of the samples have a smooth surface morphology with low roughness and low defect density. Root mean square (rms) roughness values were determined as 0.70, 0.32, and 0.31 nm for sample A, B, and C, respectively. Since the surface is strongly influenced by the layers beneath it, (rms) roughness values can be considered as the interface parameter (lateral dimension) used to calculate the mobility limited by interface roughness scattering.

HR-XRD measurements were done to determine the phases and crystal qualities of the samples. The ω-2θ scans for all three samples are shown in Fig. 3. In the spectrum, the diffraction peaks corresponding to (002) plane of the GaN layers were observed at 34.501º, 34.506º, and 34.524º for samples A, B, and C respectively. Diffraction peaks observed at 35.725º, 35.694º, and 35.702º are due to (002) plane of the $Al_xIn_yGa_{1-x-y}N$ epilayers for samples A, B, and C, respectively.

Al, In, and Ga contents in $Al_xIn_yGa_{1-x-y}N$ epilayers were determined by XPS and HR-XRD by applying 2θ-scan simulations on measured diffraction patterns. The contents were found to be approximately 88.3% (Al), 3.2% (In), and 8.5% (Ga) for sample A. The other two samples have also almost the same composition content in their respective barrier layers.

The dislocation densities (screw and edge), representing the crystal quality of samples can be deduced from the full width at half maximums (FWHM) of the rocking curves (*i.e.* the symmetrical (002) and asymmetrical (102) plane reflections) [39]. The total (edge and screw) dislocation densities were calculated as 2.44×10^8, 2.31×10^8 and 2.22×10^8 cm^{-2} for sample A, B and C, respectively. These data were used to calculate the mobilities constrained by the dislocation scattering.

The temperature dependent Hall measurements were carried out at a magnetic field of 0.5 T between 12-350 K temperature range using standard square Van der Pauw geometry. Hall mobilities, sheet carrier densities and resistances obtained from Hall measurements at low and room temperature and the barrier thicknesses obtained from SEM are given in Table I.

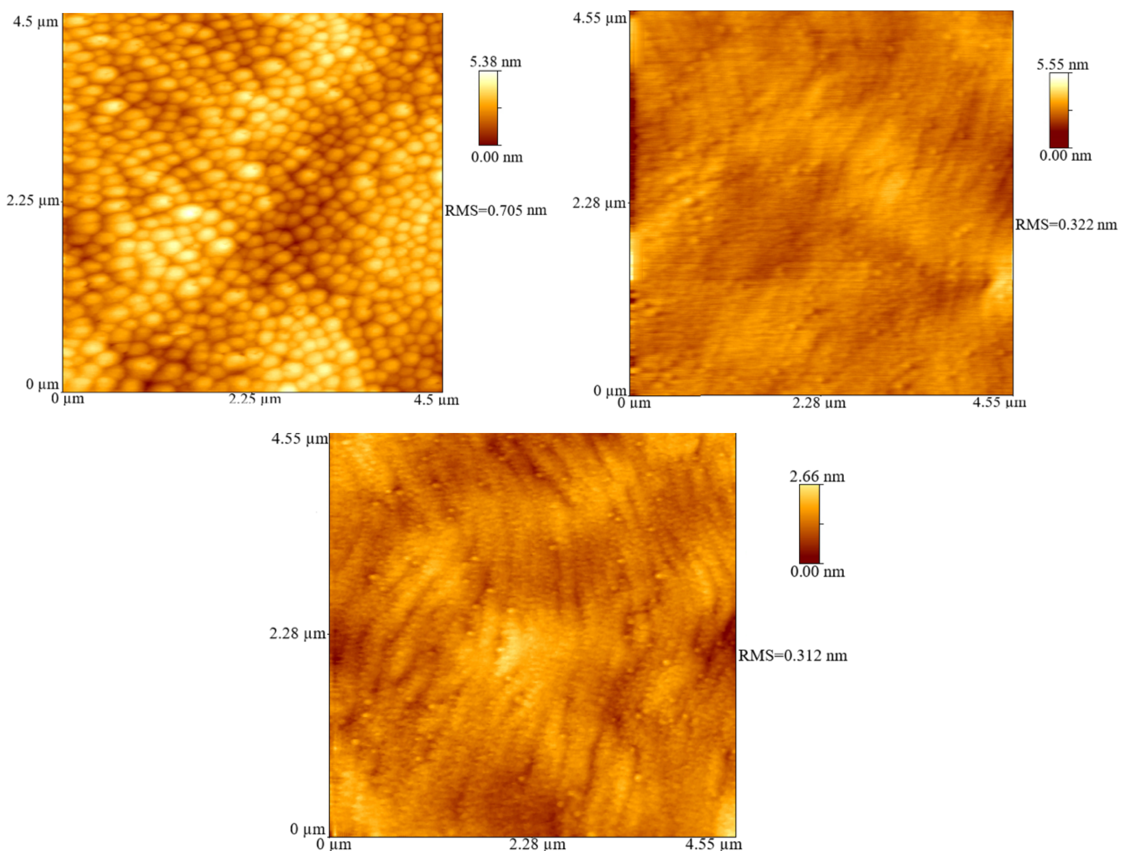

Fig. 2. AFM images of sample A, B and C respectively.

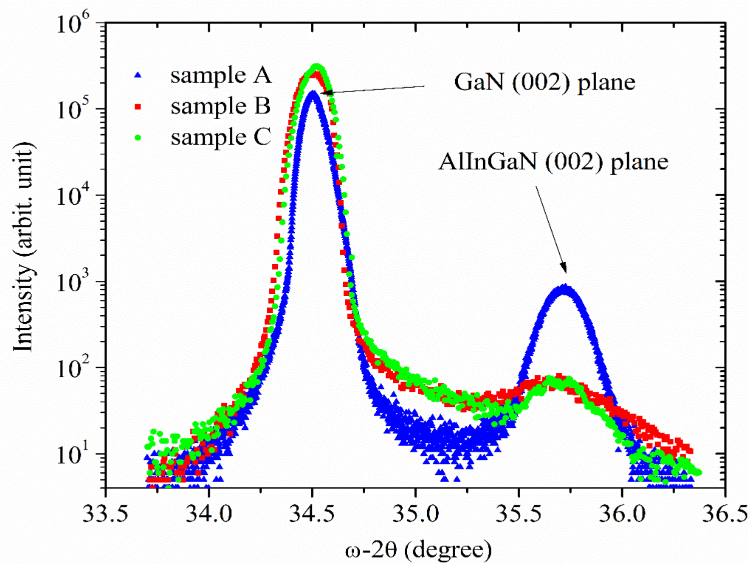

Fig. 3. HR-XRD ω–2θ scan spectra of AlxInyGa1-x-yN/GaN heterojunction structure grown on sapphire substrate.

TABLE I: HALL MOBILITY, SHEET CARRIER DENSITY, SHEET RESISTANCE AT 12 K AND 300 K TEMPERATURE

AlInGaN Thickness (nm)	Mobility $(cm^2V^{-1}s^{-1})$		Sheet Carrier Density ($\times 10^{13}$ cm^{-2})		Sheet Resistance (Ω/)	
	12K	300K	12K	300K	12K	300K
37.2	1,161	419	0.37	0.77	1,455	1,937
10.6	883	492	3.86	4.43	183	287
4.30	876	452	1.74	2.13	410	649

The sheet carrier densities and sheet resistances as a function of temperature are given in Fig. 4. The sheet carrier densities for all samples increase monotonically at different rates as the temperature increases, probably due to the temperature-induced thermal excitation of impurities in bulk GaN and AlInGaN barrier layers [40].

This temperature behavior implies that total conduction could be the combination of both 3D and 2D transport of carriers. Therefore, temperature dependent mobilities and carrier densities from bulk and 2D channels were first separated using an approach called as Parallel Conduction Extraction Method (SPCEM) [41]. Then, the main scattering mechanisms, including acoustic and optical phonon, dislocation alloy disorder, and interface roughness, which determine the total mobility via the Matthiessen rule [44] were applied to the extracted Hall mobility data. The calculations details are given in [42], [43]. The parameters used in calculations are taken from [6] and given in Table II.

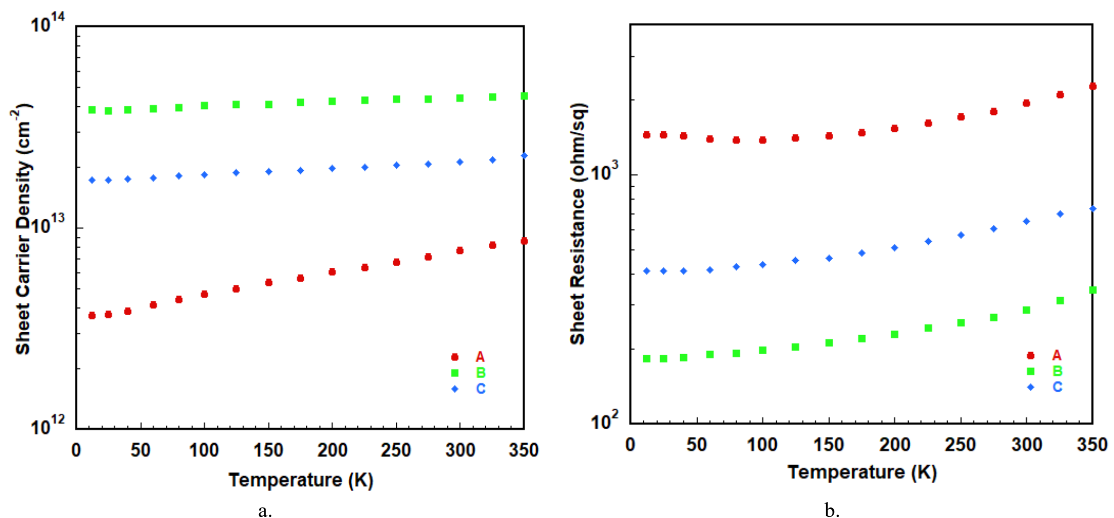

Fig. 4. a) Sheet carrier densities and; b) corresponding sheet resistance of samples as a function of temperature.

TABLE II: SOME PARAMETERS OF GaN USED TO CALCULATE THE SCATTERING MECHANISMS

Electron effective mass (m_0)	$m^* = 0.22$
High frequency dielectric constant (ε_0)	$\varepsilon_\infty = 5.35$
Static dielectric constant (ε_0)	$\varepsilon_s = 8.9$
LO-phonon energy (meV)	$\hbar\omega = 92$
Longitudinal acoustic phonon Velocity (m/s)	$\upsilon_L = 6.56 \times 10^3$
Density of the crystal (kg/m^3)	$\rho = 6.15 \times 10^3$
Deformation potential (eV)	$E_D = 8.3$
The electromechanical coupling coefficient	$K^2 = 0.039$
Electron wave vector (m^{-1})	$k = 7.27 \times 10^8$
Effective Bohr radius in the material (Å)	$a_B = 23.1$
Lattice constant in the (0001) direction (Å)	$c_0 = 5.185$
The 2D Thomas Fermi wave vector (m^{-1})	$q_{TF} = 8.68 \times 10^8$

The temperature-dependent Hall and calculated mobilities are shown in Fig. 5. Comparison of the mobilities and carrier densities measured at room temperature is also given in the Fig. 5 As can be seen from the Fig. 5, the measured Hall mobilities decrease at different rates as the temperature increases. The calculated total mobilities match the experimental results quite well for all samples. This agreement reveals that Hall mobilities are predominantly determined by interface roughness scattering at low and moderate temperatures. It has been observed that optical and acoustic phonon scattering together with the interface roughness above 250 K are collectively effective in determining the overall mobilities for all sample with different strengths. The influence of the optical phonon component on the total mobility increases with increasing temperature and reaches an almost similar strength with interface roughness scattering above room temperature. Since interface roughness scattering (IFR) is the predominant scattering mechanisms, it should be investigated in detail. IFR scattering strongly depends on the roughness between the well and barrier interface where the tow-dimensional electron gas formed [45]. Since the roughness can only be estimated by experiments, it must be carefully included into the carrier transport calculations.

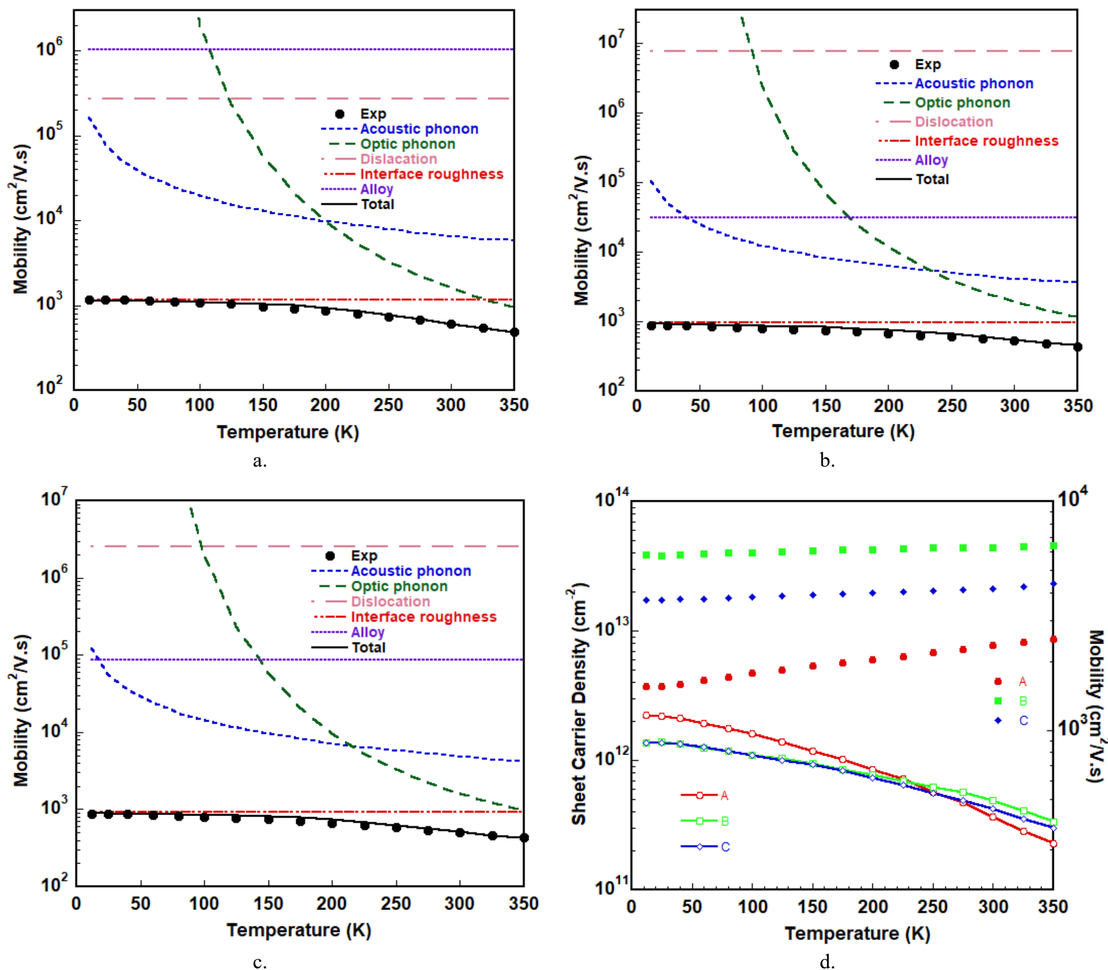

Fig. 5. The measured and calculated mobilities including major scattering mechanisms for sample: a) A; b) B; and c) C; d) Comparison of room temperature mobilities and carrier densities.

In general, there are two parameters known as the correlation length Λ and the lateral size Δ (roughness height) at the heterointerface used to calculate the mobility limited purely by interface roughness scattering. The mobility limited by IFR scattering increases as Δ decreases and Λ increases. In the mobility calculation, since the surface roughness of the barrier layer is assumed to mimic the roughness of the AlInGaN/GaN interface layer, the rms roughness values obtained from the AFM scans were used as the lateral dimension parameter (Δ). Therefore, Δ parameters were used as 0.70, 0.32, and 0.31 nm for sample A, B, and C, respectively. However, the correlation length was taken as a free parameter in the range of 5-30 nm [46] to fit the experimental data.

Considering the structural parameters and growth conditions obtained from the measurements, it is seen that the only difference between these three samples is the thickness of the AlInGaN barrier layer. In a theoretical study reported in the literature [47], it was shown that as the AlInGaN barrier thickness increases, the mobility and sheet carrier density increase. However, no clear correlation was observed between the sheet carrier density and the thickness of the barrier layers in our samples. The room temperature Hall mobility and the sheet carrier density of sample C with 4.30 nm barrier thickness are $452\ cm^2/V.s$ and $2.13\times10^{13}\ cm^{-2}$, respectively. They increase to $492\ cm^2/V.s$ and $4.43\times10^{13}\ cm^{-2}$ for sample B with a larger barrier thickness of 10.6 nm. Although the carrier density of sample B is about twice that of sample C, their mobility is close at room temperature. Sample A, which has the largest barrier thickness of 37.2 nm among the samples, has the lowest carrier density with $0.77\times10^{13}\ cm^{-2}$ and corresponding mobility of $419\ cm^2/V.s$. These differences observed in sheet carrier density of samples with different AlInGaN layer thicknesses may be due to strain relaxation, which reduces the charges induced by piezoelectric polarization at the heterointerface. The sheet carrier density affects the strength of the scattering mechanics differently. Increasing the carrier density increases the mobility limited by optical phonon scattering while decreasing the mobility limited by IFR and acoustic phonon scattering. The fact that these three scattering mechanisms are effective at different strengths may explain the results observed in our samples.

IV. Conclusion

The transport properties of a quaternary $Al_xIn_yGa_{1-x-y}N$/GaN heterojunction with three different barrier layer thicknesses of 37.2, 10.6 and 4.30 nm were determined using Hall measurements in the temperature range of 12-350 K. The effect of the AlInGaN epilayer thickness on measured mobilities and sheet carrier densities was discussed within the framework of major scattering mechanisms including optical phonon, acoustic phonon (through both deformation potential and piezoelectric), dislocation, alloy disorder and interface roughness. The sample parameters, some of which are used in the calculation of scattering rates, have been obtained by various characterization techniques. It has been realized that scattering due to interface roughness limits electron mobility in all samples at low and medium temperatures. As the temperature rose toward room temperature and above, predominantly optical, and less effectively acoustic phonon scatterings came into play together, along with the IFR, in the determining total mobilities of the samples. All samples were claimed to suffer from poor interface quality, particularly the correlation length Λ with higher carrier densities.

References

[1] Morkoç H. *Handbook of Nitride Semiconductors and Devices.* vols I–III (New York: Wiley) 2008.

[2] Xie J, Leach J H, Ni X, Wu M, Shimada R, Özgür Ü, Morkoç H. Electron mobility in InGaN channel heterostructure field effect transistor structure with different barriers. *Appl. Phys. Lett*, 2007; 91:262102. https://doi.org/10.1063/1.2824461.

[3] Miyoshi M, Egawa T, Ishikawa H, Asai K-I, Shibata T, Tanaka M and Oda O. Nanostructural characterization and two dimensional electron-gas properties in high-mobility AlGaN/AlN/GaN heterostructures grown on epitaxial AlN/sapphire templates. J. Appl. Phys, 2005;98:063713. https://doi.org/10.1063/1.2060946.

[4] Xie J, Ni X, Wu M, Leach JH, Özgür Ü, Morkoç H. High electron mobility in nearly lattice-matched AlInN/AlN/GaN heterostructure field effect transistors. *Appl. Phys. Lett*, 2007;91:132116. https://doi.org/10.1063/1.2794419.

[5] Berdalovic I, Poljak M, Suligoj T. A comprehensive model and numerical analysis of electron mobility in GaN-based high electron mobility transistors. *J. Appl. Phys*, 2021;129: 064303. https://doi.org/10.1063/5.0037228.

[6] Lisesivdin SB, Acar S, Kasap M, Ozcelik S, Gokden S, Ozbay E. Scattering analysis of 2DEG carrier extracted by QMSA in undoped $Al_{0.25}Ga_{0.75}N$/GaN heterostructures. *Semicond. Sci. Technol*, 2007;22:543. https://doi.org.10.1088/0268-1242/22/5/015.

[7] Smorchkova, IP, Chen L, Mates T, Shen L, Heikman, S, Moran B, Keller S, *et al.* AlN/GaN and (Al,Ga)N/AlN/GaN two-dimensional electron gas structures grown by plasma-assisted molecular-beam epitaxy. *Journal of Appl. Phys*, 2001;90:5196. https://doi.org/10.1063/1.1412273.

[8] Jeganathan K, Ide T, Shimizu M, Okumura H. Two-dimensional electron gases induced by polarization charges in AlN/GaN heterostructure grown by plasma-assisted molecular-beam epitaxy. *Journal of Appl. Phys*, 2003;94: 3260, https://doi.org/10.1063/1.1599979.

[9] Miyoshi M, Egawa T, Ishikawa H. Study on mobility enhancement in MOVPE-grown AlGaN/AlN/GaN HEMT structures using a thin AlN interfacial layer. *Solid-State Electronics,* 2006;50:1515. https://doi.org/10.1016/j.sse.2006.07.016.

[10] Cao Y, Jena D. High-mobility window for two-dimensional electron gases at ultrathin AlN/GaN heterojunctions. *Appl. Phys. Lett*, 2007;90:182112. https://doi.org/10.1063/1.2736207.

[11] Kuzmík J. Power Electronics on InAlN/(In)GaN: Prospect for a record performance. *IEEE Electron Device Lett*. 2001;22:510. https://doi.org/10.1109/55.962646.
[12] Kuzmík J. InAlN/(In)GaN high electron mobility transistors: some aspects of the quantum well heterostructure proposal. Semicond. *Sci. Technol*, 2002;17:540, https://doi.org/10.1088/0268-1242/17/6/307.
[13] Katzer DS, Storm DF, Binari SC, Shanabrook BV, Torabi A, Zhou L, Smith DJ. Molecular beam epitaxy of InAlN/GaN heterostructures for high electron mobility transistors. *J. Vac. Sci. Technol. B*, 2005;23:1204. https://doi.org/10.1116/1.1927103.
[14] Gonschorek M, Carlin J-F, Feltin E, Py MA, ve Grandjean N. High electron mobility lattice-matched AlInN/GaN field-effect transistor heterostructures. *Appl. Phys. Lett*, 2006; 89: 062106. https://doi.org/10.1063/1.2335390.
[15] Tulek R, Ilgaz A, Gokden S, Teke A, Ozturk MK, Kasap M, *et al.* Comparison of the transport properties of high quality AlGaN/AlN/GaN and AlInN/AlN/GaN two-dimensional electron gas heterostructures. *J. Appl. Phys*, 2009;105:013707. https://doi.org/10.1063/1.2996281.
[16] Teke A, Gökden S, Tülek R, Leach JH, Fan Q, Xie J, *et al.* The effect of AlN interlayer thicknesses on scattering processes in lattice-matched AlInN/GaN two-dimensional electron gas heterostructures. *New Journal of Physics*, 2009;11: 063031. https://doi.org/10.1088/1367-2630/11/6/063031.
[17] Xie J, Ni X, Wu M, Leach JH, Özgür Ü, Morkoç H. High electron mobility in nearly lattice-matched AlInN/AlN/GaN heterostructure field effect transistors. *Appl. Phys. Lett*, 2007; 91:132116. https://doi.org/10.1063/1.2794419.
[18] Gökden S, Tülek R, Teke A, Leach JH, Fan Q, Xie J, *et al.* Mobility limiting scattering mechanisms in nitride-based two-dimensional heterostructures with InGaN channel, *Semicond. Sci. Technol*, 2010;25:045024. https://doi.org/10.1088/0268-1242/25/4/045024.
[19] Xie J, Leach JH, Ni X, Wu M, Shimada R, Özgür Ü, Morkoç H. Electron mobility in In GaN channel heterostructure field effect transistor structures with different barriers. *Appl. Phys. Lett*, 2007;91:262102. https://doi.org/10.1063/1.2824461.
[20] Okamoto N, Hoshino K, Hara N, Takikawa M, Arakawa Y. MOCVD-grown InGaN-channel HEMT structures with electron mobility of over 1000 cm^2/V.s. *Journal of Crystal Growth*, 2004; 272:278. https://doi.org/10.1016/j.jcrysgro.2004.08.071.
[21] Tülek R, Arslan E, Bayraklı A, Turhan S, Gökden S, Duygulu Ö, Kaya AA. *et al.* The effect of GaN thickness inserted between two AlN layers on the transport properties of a lattice matched AlInN/AlN/GaN/AlN/GaN double channel heterostructure. *Thin Solid Films*, 2014;551:146. https://doi.org/10.1016/J.TSF.2013.11.114.
[22] Zhang S, Li MC, Feng ZH, Liu B, Yin JY, Zhao C. High electron mobility, and low sheet resistance in lattice-matched AlInN/AlN/GaN/AlN/GaN double-channel heterostructure. *Appl. Phys. Lett*, 2009;95:212101. https://doi.org/10.1063/1.3264961.
[23] Zhang S, Yin J Y, Feng Z H, Li M C, Wanga J Z, and Zhaoa L C. Highly uniform sheet resistance of the double-channel AlInN/GaN heterostructure. Superlattice. Microst, 2010;48:523. https://doi.org/10.1016/j.spmi.2010.09.004.
[24] Liu Y, Jiang H, Arulkumaran S, Egawa T, Zhang B, and Ishikawa H. Demonstration of undoped guaternary AlInGaN heterostructure field effect transistor on sapphire substrate. Applied Physics Letters, 2005;86:223510. https://doi.org/10.1063/1.1942643.
[25] Takamaya T, Yuri M, Itoh K, Baba T, Harris JS. Analysis of phase separation region in wurtzite group in nitride quaternary material system using modified valance force field model. *J. Cryst. Growth*, 2001;222:29. https://doi.org/10.1016/S0022-0248(00)00869-1.
[26] Hahn H, Reuters B, Wille A, Ketteniss N, Benkhelifa F, Ambacher O, Kalisch H, *et al.* First polarization-engineered compressively strained AlInGaN barrier enhancement-mode MISHFET. Semicond. *Sci. Technol*, 2012;27:055004. https://doi.org/10.1088/0268-1242/27/5/055004.
[27] Wang R, Li G, Verma J. 220-GHz Quaternary Barrier InAlGaN/GaN HEMTs. *IEEE Electron Device Letters*, 2011;32:1215. https://doi.org/10.1109/LED.2011.2158288.
[28] Lecourt F, Agboton A, Ketteniss N. Power Performance at 40 GHz Quaternary Barrier InAlGaN/GaN HEMT. *IEEE Electron Device Letter*s, 2013;34:978. https://doi.org/10.1109/LED.2013.2266123.
[29] Wang R, Li G, Karbasian G. Quaternary Barrier InAlGaN/GaN HEMTs with ft/fmax 230/300 GHz. *IEEE Electron Device Letter*s, 2013;34:378. https://doi.org/10.1109/LED.2013.2238503.
[30] Liu Y, Egawa T, Ishikawa H, Jimbo T. High quality quaternary AlInGaN epilayers on sapphire. *Phys. Status Solidi A*, 2003;200:36. https://doi.org/10.1002/pssa.200303469.
[31] Liu Y, Egawa T, and Jiang H. Enhancement-mode quaternary AlInGaN/GaN HEMT with non-recessed-gate on sapphire substrate. *Electron. Lett*, 2006;42:884. https://doi.org/10.1049/el:20061150.
[32] Li Y, Zhang J, Wan W, Zhang Y, and Nie Y. Alloy disorder scattering limited mobility of two-dimensional electron gas in the quaternary AlInGaN/GaN heterojunctions. *Physica E*, 2015;67:77. https://doi.org/10.1016/j.physe.2014.11.009.
[33] Zhang J, Yang X, Cheng J, Feng Y. Enhanced transport properties in InAlGaN/AlN/GaN heterostructures on Si (111) substrates: The role of interface quality. *Applied Physics Letters*, 2017;110:172101. https://doi.org/10.1063/1.4982597.
[34] Liu T, Jiao S, Wang D, Zhao L, Yang T, Xiao Z. Growth and characterization of quaternary AlInGAN multiple quantum wells with different Al composition. *Applied Surface Science*, 2014;301:178. https://doi.org/10.1016/j.apsusc.2014.02.034.
[35] Lee S-N, Paek HS, Kim H, Kim KK. Growth and characterization of AlInGAN protective layer to suppress the thermal damage of InGaN multiple quantum well. *Journal of Crystal Growth*, 2008;310:3881. https://doi.org/10.1016/j.jcrysgro.2008.05.056.
[36] Sonmez F, Arslan E, Ardali S, Tiras E, Ozbay E. Determination of scattering mechanisms in AlInGaN/GaN heterostructures grown on sapphire substrate. *Journal of Alloys and Compounds*, 2021;864:158895. https://doi.org/10.1016/j.jallcom.2021.158895.
[37] Lecourt F, Agboton A, Ketteniss N, Behmenburg H, Defrance N, Hoel V. et al. Power performance at 40 GHz on quaternary barrier InAlGaN/GaN HEMT. IEEE Electron Device Lett, 2013;34:978. https://doi.org/10.1109/LED.2013.2266123.
[38] Liu Y, Jiang H, Arulkumaran S, Egawa T, Zhang B, Ishikawa H. Demonstration of undoped quaternary AlInGaN⁄GaN heterostructure field-effect transistor on sapphire substrate. *Appl. Phys. Lett*, 2005;86:223510. https://doi.org/10.1063/1.1942643.
[39] Arslan E, Ozturk M K, Teke A, Ozcelik S, and Ozbay E. Buffer optimization for crack- free GaN epitaxial layers grown on Si(1 1 1) substrate by MOCVD. J. Phys. D Appl. Phys, 2008;41:155317. https://doi.org/10.1088/0022-3727/41/15/155317.
[40] Lisesivdin SB, Yildiz A, Acar S, Kasap M, Ozcelik S, Ozbay E. Electronic transport characterization of AlGaN⁄GaN heterostructures using quantitative mobility spectrum analysis. *Appl. Phys. Lett*, 2007;91:102113. https://doi.org/10.1063/1.2778453.
[41] Lisesivdin SB, Balkan N, Ozbay E. A simple parallel conduction extraction method (SPCEM) for MODFETs and undoped GaN-based HEMTs. *Microelectronics Journal*, 2009;40:413. https://doi.org/10.1016/j.mejo.2008.06.006.
[42] Gokden S, Baran R, Balkan N, Mazzucato S. The effect of interface roughness scattering on low field mobility of 2D electron gas in GaN/AlGaN heterostructure. *Physica E*, 2004;24:249. https://doi.org/10.1016/j.physe.2004.04.042.
[43] Gokden S, Ilgaz A, Balkan N, Mazzucato S. The effect of scattering mechanisms on the low field mobility in GaN/AlGaN heterostructures. *Physica E*, 2004;25:86. https://doi.org/10.1016/j.physe.2004.06.038.
[44] Ridley BK, Foutz BE, Eastman LF. Mobility of electrons in bulk GaN and AlxGa1−xN/GaN heterostructures. *Phys. Rev. B*, 2000;61:16862. https://doi.org/10.1103/PhysRevB.61.16862.

[45] Saha S, Kumar J. Role of interface roughness scattering, temperature, and structural parameters on the performance characteristics of III-nitride quantum cascade detectors. *J. Appl. Phys*, 2017;121:053104. https://doi.org/10.1063/1.4975481.
[46] Çörekçi S, Usanmaz D, Tekeli Z, Çakmak M, Özçelik S, Özbay E. Surface Morphology of AlGaN/Al_2O_3-High Electron Mobility Transistor Structure. *J. Nanosci. Nanotechnol*, 2008;8:640. https://doi.org/10.1166/jnn.2008.a181.
[47] Li Y, Zhang J, Liu G, Quan R, Duan X, Zhang J, and Hao Y. Theoretical analysis of the mobility of two-dimensional electron gas in the quaternary $Al_xIn_yGa_{1-x-y}N$/GaN heterojunctions limited by the alloy composition fluctuation. *AIP Adv*, 2017;7:105109. https://doi.org/10.1063/1.4985825.